

Formation of microscopic internal stresses in rails during long-term operation

V. E. Gromov, Dr. Phys.-Math., Prof., Head of the Dept. of Natural Sciences named after prof. V. M. Finkel¹, e-mail: gromov@physics.sibsiu.ru;

M. A. Porfiryev, Researcher¹, e-mail: mporf372@gmail.com;

R. E. Kryukov, Cand. Eng., Associate Prof., Dept. of Metallurgy of Ferrous Metals¹, e-mail: rek_nzrmk@mail.ru;

V. V. Shlyarov, Postgraduate Student, Dept. of Natural Sciences named after prof. V. M. Finkel¹, e-mail: shlyarov@mail.ru

¹ Siberian State Industrial University (Novokuznetsk, Russia)

The level of microscopic internal long-range stress fields σ_l on the rolling surface and the working fillet is determined for two categories of rails with a carbon content of 0.74 wt. % and 0.91 wt. %. DT350 for general purpose and DT400IK of increased wear resistance and contact endurance after the passed tonnage of 1,770 mln. t (for DT350) and 187 mln. t DT400IK (1) and 234 mln. t of DT400IK (2). For this purpose, the bending extinction contours were analyzed by means of transmission electron diffraction microscopy, the parameters of which were used in calculating σ_l . The presence of excess extinction contours indicates the bending-torsion of the lattice, which is characterized by the excess density of dislocations. A comparison is made with other methods for measuring internal stress fields at the meso- and macro levels. It is shown that the parameters of the bending extinction contours are the most informative and allow one to control the locality of the measurement σ_l . Sources of internal stress fields in rail steels are noted. An increase in the level of σ_l was revealed in DT400IK rails in comparison with DT350 rails. The growth of the passed tonnage for rails of category DT400IK leads to an increase in σ_l , the values of internal stresses on the fillet surface exceed the corresponding values on the rolling surface. The physical causes of the observed changes are discussed.

Keywords: internal stress fields, excess dislocation density, surface, rails, electron microscopy.

DOI: 10.17580/cisisr.2023.02.15

Introduction

Production of long-length (100 m) differentially hardened general-purpose rails of DT350 category was launched in Russia 10 years ago, and three years ago – rails with increased wear resistance and contact endurance (rails of DT400IK category) for operation in straight track sections at speeds up to 200 km/h and curved track sections without restrictions on traffic density. According to Russian Railways, up to 75 % of rails were replaced in 2020 due to their wear limit state and contact fatigue defects. These processes are largely determined by the formation of internal stress fields.

The problem of internal stresses in metals and alloys has been at the center of attention of researchers for many years [1–3]. This is explained by the fact that internal stresses play an important role in the formation of the yield stress, strain hardening [4–7] and especially in the fracture of crystalline materials, namely, in the initiation and opening of microcracks [8–11]. Their role is great in the evolution of the defect structure in various types of heat treatment of metals, alloys, and steels [12]. In addition, internal stresses play a significant role in phase and structural transformations [2, 3, 12, 13]. And, finally, the effect of internal stresses in the production of bulk nanostructured materials by the method of severe plastic deformation cannot be disregarded [14–16].

Internal stresses are classified, first of all, according to the area of their localization, and macro-, meso- and microstresses are distinguished. Macro stresses are localized in the entire sample or in a significant part of its volume. Mesoscopic internal stresses are localized in volumes ranging from tens to hundreds of micrometers. In polycrystals, meso stresses are localized in the volumes of one or several grains or in a part of the grain volume. Microscopic stress fields are localized in areas of a few micrometers or less.

The existing methods for assessing internal stresses can be divided into 2 groups: destructive and non-destructive. Destructive methods can conditionally be divided into: chemical, thermal, metallochemical and mechanical [17]. The use of destructive methods for assessing internal stresses leads to partial or complete destruction of the product. All destructive methods for detecting and measuring internal stresses in products relate to stresses of the I type, which mainly determine the operational properties of products.

Non-destructive methods include magnetic, optical, and polarization-optical ones [18]. These methods make it possible to measure elastic deformations inside the part without changing its geometry. However, non-destructive methods, like destructive ones, are integral. The averaging area of stresses (stresses of the I type) with the use of these methods is centimeters.

Internal stresses can be determined using X-ray diffraction analysis (measurement of stresses of the I and II types), which also refers to non-destructive methods [19, 20]. The averaging area of stresses in this case decreases significantly and amounts to millimeters but remains large as before. It is possible to estimate the amplitude of mesoscopic internal stresses [21–23].

At present, the most informative method for studying meso- and microscopic fields of internal stresses is diffraction electron microscopy, which allows the locality of internal stresses measurements over a wide range to be controlled (from hundreds of nanometers to hundreds of microns) [24]. Since in the work we use the method of transmission electron microscopy, only this method will be considered below.

The values of meso- and microscopic internal stresses are reconstructed from the material structure in several ways: 1) by the bending radius of dislocation in the slip plane [14], 2) by the distance between dislocations and the parameters of dislocation clusters, 3) by the distance between active slip planes and, finally, 4) by the parameters of extinction bend contours [11, 24].

The purpose of this work is to study the internal stresses in the rail surface after operation and their sources by the method based on the analysis of extinction bend contours.

Materials and methods

Samples of 100-meter differentially hardened rails of DT350 and DT400IK categories after operation were used as research materials. The passed tonnage for rails DT350 is 1,770 mln. t gross, for rails DT400IK (1) – 187 mln. t on the experimental ring of Russian Railways, and for rails DT400IK (2) – 234 mln. t on the Trans-Baikal Railway. They were made of steels E76KhF and E90KhAF (for DT350 and DT400IK, respectively), the elemental composition of which is regulated by Russian National Standard 51685-243 and Technical Specification 24.10.75111-298-057576.2017RZD. The dislocation substructure was determined by transmission electron microscopy (TEM) (microscope JEOL JEM2100F) [24].

Rails were studied along the central axis of symmetry (rolling surface) and along the rounding radius (working fillet) of the rail head at distances of 0, 2 and 10 mm from the surface.

The curvature-torsion of crystal lattices χ , scalar ρ , excess density of dislocations ρ_{\pm} and stress fields σ_l were estimated on the rolling surface along the central axis and rounding radius of the fillet.

Results and discussion

Determination of internal stresses by TEM

The uncharged dislocation ensemble (i.e., an ensemble without excess dislocations) gives the internal shear stress (stress fields created by the dislocation structure) determined by the formula [3,8,12]:

$$\sigma = maGb\sqrt{\rho}, \quad (1)$$

where m – orientation factor, or the Schmid factor [12]; a – parameter depending on the type of dislocation ensemble (the value of the coefficient $a = 0.05$ –1.0 for the uncharged dislocation ensemble [3,8,11]); G – shear modulus, b – Burgers vector; ρ – scalar density of dislocations.

In the case of a charged dislocation ensemble, when there is an excess density of dislocations $\rho_{\pm} = \rho_+ - \rho_- \neq 0$, internal moment (or long-range) stresses are created. The presence of excess dislocation density and, accordingly, internal moment stresses are identified by the presence of extinction bend contours in the material.

The extinction bend contour is the result of the diffraction contrast observed in the electron microscopic image of the structure of a severely deformed crystal.

The crystal lattice bend can be [3,7,8,12,14]: a) purely elastic, created by stress fields accumulated due to deformation incompatibility, for example, polycrystal grains, material matrix and non-deformable particles; b) plastic, if the bend is created by dislocation charges, i.e. an excess density of dislocations localized in a certain volume of the material, and c) elastic-plastic, when both sources of fields are present in the material.

With the presence of extinction bend contours in the material, the TEM method can be used to measure internal (moment or long-range) stresses. It is their presence that leads to the bend of the foil (which corresponds to the curvature-torsion of the crystal lattice) if the foil retains the shape of a plate [24]. The procedure for measuring the magnitude of internal moment (long-range) stresses is reduced to determining the curvature gradient of the foil (crystal lattice):

$$\chi = \frac{\partial\varphi}{\partial l}, \quad (2)$$

where $\partial\varphi = \Delta\varphi$ – the change in the orientation of the foil reflecting plane, $\partial l = \Delta l$ – displacement of the extinction bend contour. The value $\chi = \partial\varphi/\partial l$ is determined by shifting the extinction contour by Δl at a controlled foil slope angle $\Delta\varphi$ in the microscope column using a goniometer. It was established by special experiments that the width of the contour in terms of misorientations for BCC steels is $\sim 1^\circ$ [3, 12]. This means that when the goniometer is rotated by $\Delta\varphi \approx 1^\circ$, the extinction bend contour is displaced by a distance equal to its width, that is, $\Delta l \approx l$.

To separate the cases of plastic, elastic, and elastic-plastic bend, it is necessary to compare the scalar dislocation density (ρ), measured in a local area near the extinction bend contour, with the excess dislocation density (ρ_{\pm}), measured locally along the misorientation gradient [12, 14]:

$$\rho_{\pm} = \frac{1}{b} \frac{\partial\varphi}{\partial l} = \frac{\chi}{b}. \quad (3)$$

1. If $\rho \geq \rho_{\pm}$ turns out to be in the investigated section of the foil, then the of the crystal lattice bend can be considered plastic. In this case, the amplitude of curvature-torsion of the crystal lattice, determined according to formula (2), $\chi = \chi_{pl}$, and the amplitude of internal moment stresses created by plastic bend is equal to:

$$\sigma_i^{pl} = m\alpha Gb\sqrt{\rho_{\pm}} = m\alpha Gb\sqrt{b\chi_{pl}}, \quad (4)$$

where $\alpha = 0.05-0.60$ is a parameter depending on the type of dislocation ensemble [14]. It should be noted that the value of α in formula (4) weakly depends on the metallic material and is almost completely determined by the type of the formed substructure [14].

2. If $\rho = 0$ in the studied section of the foil near the extinction bend contour, then the crystal lattice bend is purely elastic. In this case, the amplitude of the curvature-torsion of the crystal lattice, determined according to formula (2), $\chi = \chi_{el}$, and the amplitude of the internal moment stresses created by elastic bending, should be determined by the formula [12, 14]:

$$\sigma_i^{bl} = m\alpha_s Gt \frac{\partial \varphi}{\partial l} = m\alpha_s Gt \chi_{bl}, \quad (5)$$

where $\alpha_s = 1-1.5$ – Strunin coefficient [12], calculated for a dislocation ensemble composed of dislocations of the same sign; t – foil thickness.

3. Finally, if $\rho < \rho_{\pm}$ turns out to be near the extinction bend contour, then the of the crystal lattice bend is elastic-plastic, and then the value of ρ_{\pm} is a conditional value. In this case, the crystal lattice bend is divided into a plastic component, for which $\rho = \rho'_{\pm}$, and an elastic component, for which $\rho''_{\pm} = \rho_{\pm} - \rho'_{\pm}$. Then the amplitude of the torsion curvature of the crystal lattice is equal to:

$$\chi = \chi_{pl} + \chi_{el}, \quad (6)$$

where χ is calculated according to formula (2),

$$\chi_{pl} = b\rho'_{\pm} = b\rho$$

and therefore

$$\chi_{el} = \chi - \chi_{pl}. \quad (7)$$

As a result, the amplitude of internal moment (long-range) stresses is determined as:

$$\sigma_i = \sigma_i^{pl} + \sigma_i^{bl}, \quad (8)$$

where σ_i^{pl} is determined according to formula (4), and σ_i^{bl} – according to formula (5):

$$\sigma = m\alpha G\sqrt{b\chi_{pl}} + m\alpha_s Gt\chi_{bl}. \quad (9)$$

Sources of internal stresses in BCC steels

A single dislocation is already a source of internal stresses. The fields from individual dislocations extend over small distances, much smaller than the distances between the nearest dislocations [24]. Groups of dislocations are more effective sources of internal stresses. They cover the entire microlevel and create fields of much greater amplitude. These dislocation groups primarily include distributed dislocation charges (excess dislocations of the same sign) [25]. However, large groups of dislocations of the same sign are rare. More often,

the material contains inhomogeneously distributed dislocations of different signs with an excess density of dislocations. Such formations, despite internal screening, create fields of internal stresses [25].

Another type of dislocation formations, that create more significant internal stresses, are various dislocation boundaries. As a rule, they contain an unequal number of dislocations of different signs and can introduce misorientation. Their main difference is that the dislocations in the boundaries belong to different slip planes, while in the dislocation charges the dislocations are on the same or close slip planes.

Other sources of internal stresses include grain boundaries, grain intersections, ledges on grain boundaries [25, 26]. The causes of these internal stresses are, first of all, the incompatibility of deformation of neighboring grains. Such incompatibility is always present, despite the action of accommodative slip systems. The second reason is the presence of lattice dislocations embedded in grain boundaries and grain-boundary sources of dislocations. A powerful source of internal stresses are partial disclinations at grain intersection and in ledges at interphase boundaries. These are boundary intersection disclinations [27]. All these sources are sources of internal stresses of plastic origin.

The sources of internal stresses of elastic origin, which arise mainly during inhomogeneous deformation of the material, are, first of all, microcracks [3, 7, 8, 25]. Another source of internal stress is the Bain distortion [12], which occurs as a result of the curvature of the crystal lattice during $\gamma \rightarrow \alpha$ phase transformation in steels. Such stresses also arise in materials strengthened by dispersed non-deformable particles [14]. In the case of partial relaxation of these fields by multiplication and slip of dislocations, they acquire an elastic-plastic character [7, 8, 25]. Depending on the degree of their interaction with the surrounding dislocation structures, the resulting internal stresses can be of all three types. In real materials, especially after significant deformations, the fields from various sources are summed up. As a result, a complex three-dimensional field of internal stresses is formed.

Internal stresses and their sources in rail steel

Rails were studied along the central axis of symmetry (rolling surface) and along the rounding radius (working fillet) of the rail head at distances of 0, 2 and 10 mm from the surface.

In accordance with formulas (1-9), the curvature-torsion of crystal lattices χ , scalar ρ , excess dislocation density ρ_{\pm} and stress fields σ_i were evaluated on the rolling surface along the central axis and rounding radius of the fillet of DT350 rails.

The conducted studies showed that the operation of the rails resulted in a significant transformation and complication of the structure, and more intensively along the radius of the fillet. If at a distance of 10 mm from the rolling surface along the axis of symmetry, the volume fraction of lamellar pearlite is 95 % and 5 % is a ferrite-carbide mixture (destroyed pearlite), then in the surface layer the share of lamellar pearlite is only 45 %, the proportion of ferrite-carbide

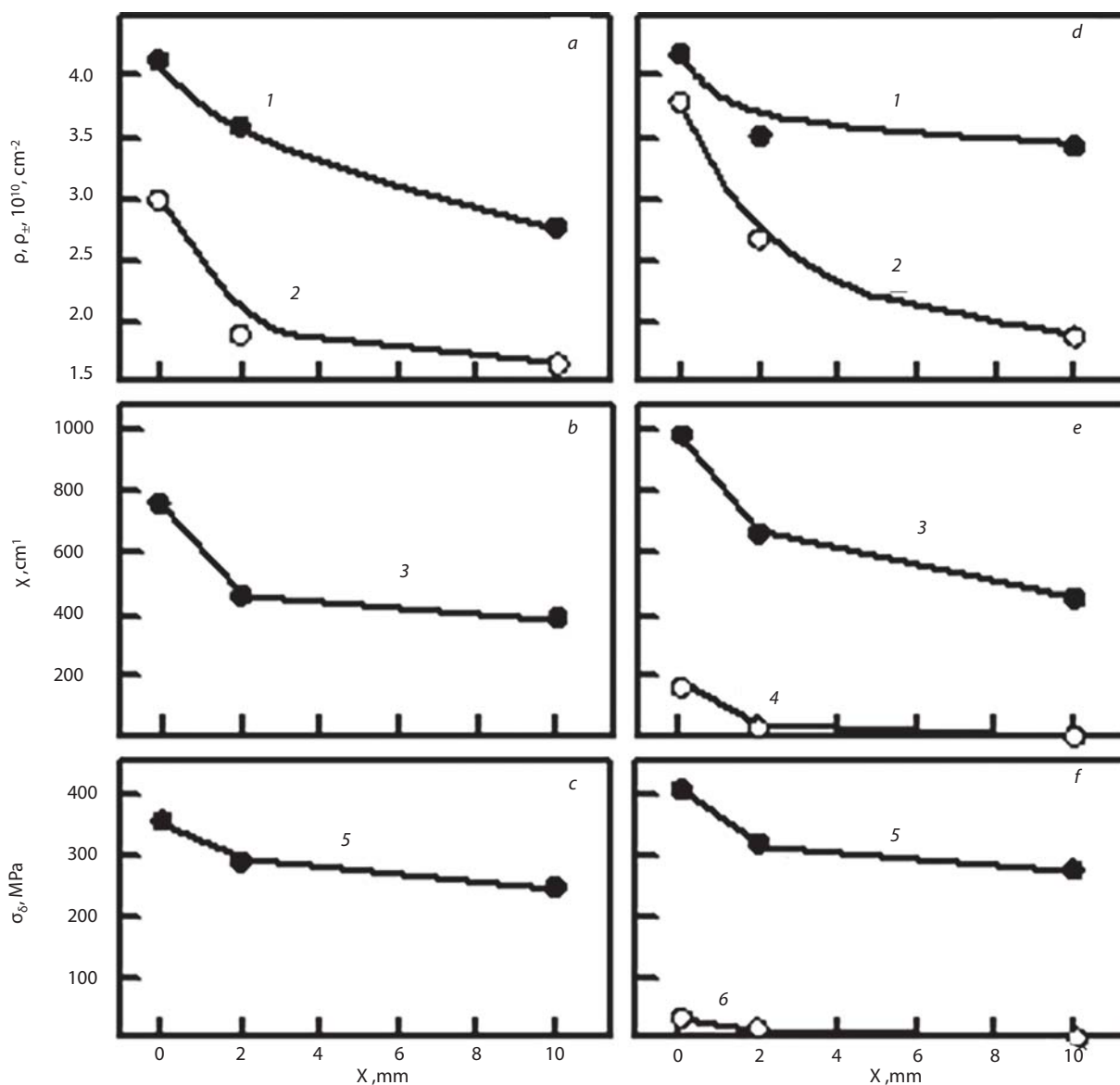


Fig. 1. Change in the average quantitative parameters of the fine structure of DT350 rails after extra-long operation with distance from the surface:

a-c – along the central axis from the rolling surface; *d-f* – along the radius of curvature of the working fillet (*a, d* – scalar ρ (1) and excess ρ_{\pm} (2) dislocation density, *b, e* – amplitude of plastic χ_{pl} (3) and elastic χ_{el} (4) curvature-torsion of crystal lattice, *c, f* – the amplitude of the internal moment plastic σ_{pl} (5) and elastic σ_{el} (6) stresses).

mixture is already 50%, and there is a fragmented structure (5%). As for the working fillet, at a distance of 10 mm from the surface along the rounding radius, the volume fraction of lamellar pearlite is also 95%, but in the surface layer it decreased to 25%, and the fraction of the fragmented structure increased to 25%. Thus, as it approaches the surface of the head, regardless of the direction of examination (along the rounding radius of the fillet or along the axis of symmetry), lamellar pearlite is gradually replaced by fractured one with the formation of a ferrite-carbide mixture and the formation of a fragmented structure, and these processes proceed more intensively in the working fillet. In Fig. 1 the changes in the quantitative parameters of the fine structure averaged over the material are shown as they approach the surface of the head.

As follows from the figure, all characteristics increase when approaching the surface of the rail head. The scalar ρ and especially the excess ρ_{\pm} dislocation density increase more intensively. However, their behavior within various structural components is different. The scalar density of dislocations in the entire material, regardless of the direction of examination (along the radius of the fillet or along the axis of symmetry), as it approaches the surface, increases at almost the same rate. The excess density of dislocations, determined from the width of the extinction bend contours, along the central axis of symmetry (rolling surface) in the entire material remains less than the scalar one ($\rho > \rho_{\pm}$), that is, plastic bending-torsion of the crystal lattice takes place: $\chi = \chi_{pl}$ and $\sigma_l = \sigma_l^{pl}$ (Fig. 1, *a-c*). The condition $\rho > \rho_{\pm}$ is also preserved along the rounding radius of the fillet in lamellar pearlite,

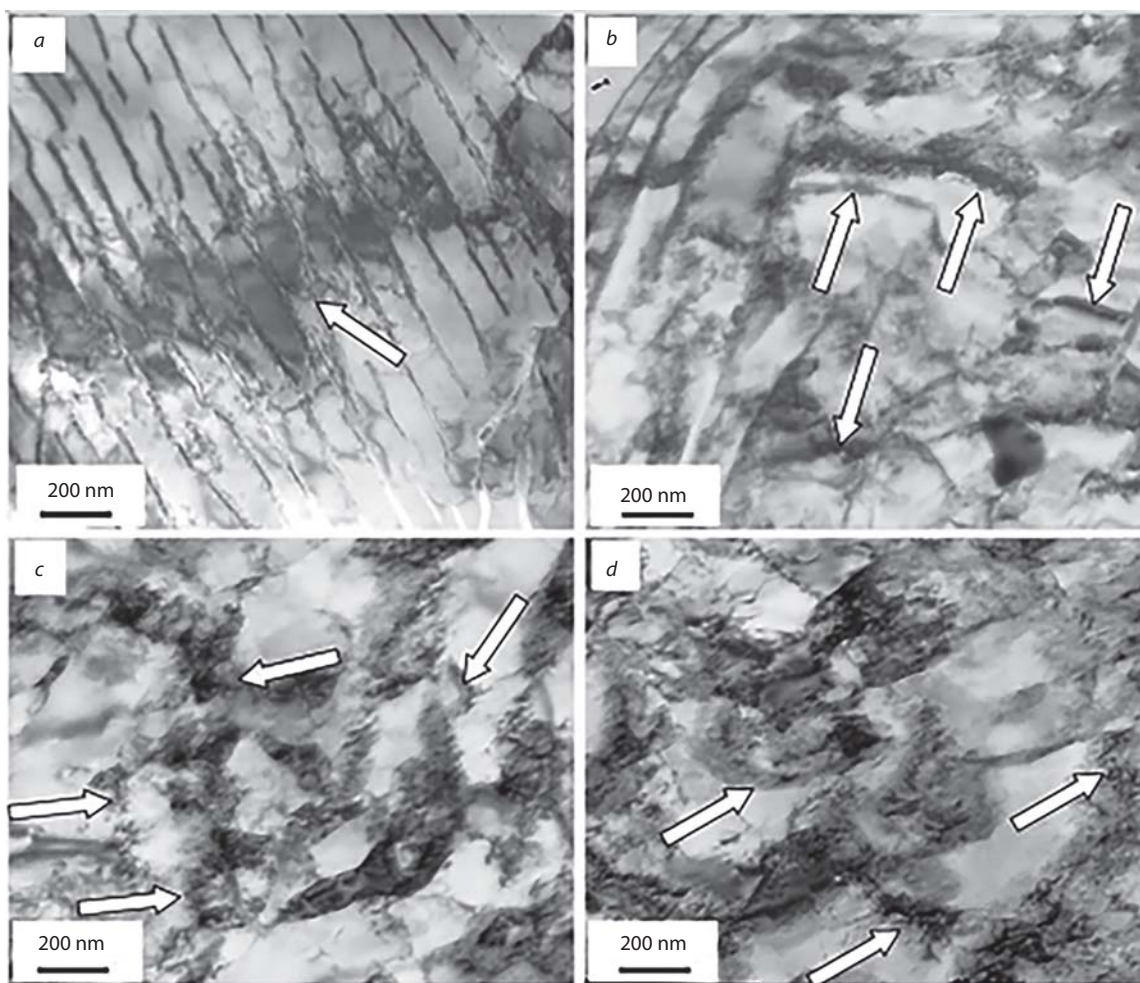


Fig. 2. TEM images of extinction bend contours (indicated by arrows) of DT350 rails in different parts of the material from different sources:
a – interface between ferrite and cementite; *b* – boundaries between fragments; *c* - globular particles at fragment boundaries; *d* – globular particles in the volume of fragments.

Parameters of stress fields in rails				
Parameter	Surface		Fillet	
	$\rho_{\pm} \cdot 10^{-10}, \text{cm}^{-2}$	σ_f, MPa	$\rho_{\pm} \cdot 10^{-10}, \text{cm}^{-2}$	σ_f, MPa
Rails				
DT400IK (1)	5.70	626	6.41	682
DT400IK (2)	8.11	891	9.21	971



Fig. 3. Cross section of the rail head, category DT400IK (2).


however, in the ferrite-carbide mixture and the fragmented structure it turns out to be $\rho = \rho_{\pm}$. This means that here the dislocation structure is completely polarized, and in these places of the material there is an elastic-plastic bending of the crystal lattice: Despite the fact that the magnitude of the elastic component is small (Fig. 1, *e, f*), it is impossible to ignore such areas in the structure of the material, since the fracture is most likely to occur in such places. Thus, the main source of internal moment (long-range) stresses in DT350 rails is the excess density of dislocations. However, there are other sources of internal stresses. Namely: ferrite and cementite interfaces, fragment boundaries and cementite particles located at the boundaries and inside the fragments. Their example is given in Fig. 2.

Table shows the parameters of stress fields on the rolling surface of DT400IK rails. The analysis of the presented results does not allow their correct comparison with the data in Fig. 1.

This may be due to the different chemical composition of rails DT350 and DT400IK (especially in terms of carbon content 0.74 wt. % and 0.91 wt. %, respectively), differen-

tial hardening modes, passed tonnage and, most importantly, operating conditions. The rails of category DT400IK after the passed tonnage already had a cross-sectional view, shown in **Fig. 3** and were withdrawn from service. It seems important that the level of internal stress fields in all cases on the fillet is higher than along the central axis of the rolling surface, which indicates the potential possibility of crack initiation in these places.

Conclusion

The analysis of sources of internal stresses occurring in bcc steels was carried out. It is shown that the entire set of sources can be conditionally divided into sources of internal stresses of plastic, elastic and elastic-plastic origin. The TEM analysis carried out for rails of DT350 category after the passed tonnage of 1770 million gross tonnes showed: 1) lamellar perlite, nearing the surface of the rail head, is gradually replaced by fractured one with the formation of a ferrite-carbide mixture and a fragmented structure, and this process occurs more intensively in the working fillet; 2) along the entire central axis of symmetry of the rail head, plastic bending-torsion of the crystal lattice takes place, along the radius of rounding of the rail head at a distance up to 2 mm – elastic-plastic; 3) the main source of internal moment stresses is the excess density of dislocations. It is shown that on the surface of the fillet the level of internal stress fields for all categories of rails after operation is higher, which indicates a potential area for initiation of microcracks. Possible physical reasons for the observed differences are discussed. 

REFERENCES

- Koneva N. A., Kozlov E. V., Trishkina L. I. Internal field sources, their screening and the flow stress. *Mat. Scie. and Eng.: A*. 2001. Vol. A319-321. pp. 156–159.
- Yang M., Pan Yu., Yuan F., Zhu Yu., Wu Back X. Stress Strengthening and Strain Hhardening in Gradient Structure. *Materials Research Letters*. 2016. Vol. 4 (3). pp. 1–8.
- Popova N. A., Ivanov Yu. F., Gromov V. E., Nikonenko E. L. et al. Internal stress in polycrystalline metallic materials. Novokuznetsk: Polygrafist, 2023. 144 p.
- Kundu A., Field D. P. Geometrically Necessary Dislocation Density Evolution in Interstitial Free Steel at Small Plastic Strains. *Metall. Mater. Trans.: A*. 2018. Vol. 49. pp. 3274–3282.
- Ivanov Yu. F., Gromov V. E., Yuriev A. A., Kormyshev V. E., Rubannikova Yu. A., Semin A. P. Deformation Strengthening Mechanisms of Rails in Extremely Long-Term Operation. *Journal of Materials Research and Technology*. 2021. Vol. 11. pp. 710–718.
- Yuriev A. A., Gromov V. E., Ivanov Yu. F., Rubannikova Yu. A., Starostenkov M. D., Tabakov P. Y. Structure and Properties of Lengthy Rails after Extreme Long-Term Operation. Materials Research Forum LLC, 2021. 193 p.
- Ivanov Yu. F., Gleser A. M., Kuznetsov R. V., Gromov V. E., Shliarova Yu. A., Semin A. P., Sundeev R. V. Fine Structure Formation in Rails under Ultra Long-Term Operation. *Materials Letters*. 2022. Vol. 309. pp. 131378.
- Smirnov A. N., Kozlov E. V. Substructure, internal stress fields and the problem of destruction of steam pipelines made of steel 12Kh1MF. Kemerovo: Kuzbassvuzizdat, 2004. 163 p.
- Panin V. E., Egorushkin V. E. Fundamental role of local curvature of crystal structure in plastic deformation and fracture of solids. *AIP Conf. Proc.* 2014. Vol. 1623. pp. 475–478.
- Cattivelli A., Roy M. J., Burke M. G., Dhers J., Jean Lee, Francis J. A. Internal stresses in a clad pressure vessel steel during post weld heat treatment and their relevance to underclad cracking. *International Journal of Pressure Vessels and Piping*. 2021. Vol. 193. pp. 104448.
- Fang X.-Y., Zhang H.-N., Ma D.-W., Wu Z.-J., Huang W. Influence of Welding Residual Stress on Subsurface Fatigue Crack Propagation of Rail. *Engineering Fracture Mechanics*. 2022. Vol. 271. pp. 108642.
- Kozlov E. V., Popova N. A., Kabanina O. V., Klimashin S. I., Gromov V. E. Evolution of the phase composition, defective structure, internal stresses and redistribution of carbon during tempering of cast structural steel. Novokuznetsk: Publishing House of SibSIU, 2007. 177 p.
- Zhang Y., Yu T., Xu R., Thorborg J., Liu W., Tischler J., Godfrey A., Jensen D. J. Local residual stresses and microstructure within recrystallizing grains in iron. *Materials Characterization*. 2022. Vol. 191. pp. 112113.
- Gleser A. M., Kozlov E. V., Koneva N. A., Popova N. A., Kurzina I. A. Plastic Deformation of Nanostructured Materials. CRC Press, Taylor & Francis Group, Boca Raton, London, New York, 2017. 321 p.
- Vinogradov A., Estrin Y. Analytical and Numerical Approaches to Modelling Severe Plastic Deformation. *Progress in Materials Science*. 2018. Vol. 95. pp. 172–242.
- Wilde G., Divinski S. Grain Boundaries and Diffusion Phenomena in Severely Deformed Materials. *Materials Transactions*. 2019. Vol. 60 (7). pp. 1302–1315.
- Burkin S. P., Shimov G. V., Andryukova E. A. Residual stresses in metal products. Yekaterinburg: Ural University Press, 2015. 248 p.
- Experimental mechanics: In 2 books: Translated from English. Ed. A. Kobayashi. M.: Mir, 1990. 616 p.
- Withers P. J. Mapping residual and internal stress in materials by neutron diffraction. *Comptes Rendus Physique*. 2007. Vol. 8 (7-8). pp. 806–820.
- Withers P. J., Turski M., Edwards L., Bouchard P. J., Buttle D. J. Recent advances in residual stress measurement. *International J. of Pressure Vessels and Piping*. 2008. Vol. 85 (3). pp. 118–127.
- McNelis K. P., Dawson P. R., Miller M. P. A Two-Scale Methodology for Determining the Residual Stresses in Polycrystalline Solids Using High Energy X-ray Diffraction Data. *J. of the Mechanics and Physics of Solids*. 2013. Vol. 61 (2). pp. 428–449.
- Demir E., Park J.-S., Miller M. P., Dawson P. R. A Computational Framework for Evaluating Residual Stress Distributions from Diffraction-Based Lattice Strain Data. *Computer Methods in Applied Mechanics and Engineering*. 2013. Vol. 265. pp. 120–135.
- Yildirim C., Jessop C., Ahlström J., Detlefs C., Zhang Y. 3D Mapping of Orientation Variation and Local Residual Stress Within Individual Grains of Pearlitic Steel Using Synchrotron Dark Field X-ray Microscopy. *Scripta Materialia*. 2021. Vol. 197. pp. 113783.
- Hirsch P. B., Howie A., Nicholson R. B., Pashley D. W., Whelan M. J. Electron microscopy of thin crystals. London: Butterworths, 1965. 570 p.
- Koneva N. A., Trishkina L. I., Zhdanov A. N., Perevalova O. B., Popova N. A., Kozlov E. V. Sources of stress fields in deformed polycrystals. *Fizicheskaya mezomekhanika*. 2006. Vol. 9 (3). pp. 93–101.
- Gromova A. V., Yuriev A. B., Ivanov Yu. F., Chinokalov V. Ya. Formation of long-range stress fields during wire drawing. *Izv. vuzov. Chernaya metallurgiya*. 2006. No. 2. pp. 27–31.
- Rybin V. V. Patterns of the formation of mesostructures during the development of plastic deformation. *Voprosy materialovedeniya*. 2002. Vol. 29 (1). pp. 11–33.